

Effects of Boundaries on Pattern Formation: Catalytic Oxidation of CO on Platinum

M. D. Graham,* Ioannis G. Kevrekidis,† K. Asakura, J. Lauterbach, K. Krischer, H.-H. Rotermund, G. Ertl

The effect of boundaries on pattern formation was studied for the catalytic oxidation of carbon monoxide on platinum surfaces. Photolithography was used to create microscopic reacting domains on polycrystalline foils and single-crystal platinum (110) surfaces with inert titanium overlayers. Certain domain geometries give rise to patterns that have not been observed on the untreated catalyst and bring to light surface mechanisms that have no analog in homogeneous reaction-diffusion systems.

Nonlinear reaction-diffusion systems can spontaneously form a wealth of spatiotemporal patterns, ranging from Turing patterns and spiral waves to “chemical turbulence” (1–4). In these systems, as in essentially every nonlinear pattern-forming system (for example, hydrodynamics), the size of the domain is an important factor. From the theoretical point of view, the ratio of the geometric domain size to some intrinsic length scale plays a central role in the study of instability and pattern formation.

We used microlithography to create a variety of reactive domains of controlled size and shape on Pt surfaces. In these microdesigned domains, we study pattern formation in the isothermal, low-pressure ($\leq 10^{-3}$ mbar) heterogeneous catalytic oxidation of CO on polycrystalline Pt and on a Pt(110) single-crystal surface. In the absence of boundaries, this system (which is strictly two-dimensional) exhibits solitary pulses, spiral waves, and target patterns (5–7) in accordance with established two-dimensional reaction-diffusion phenomenology [for example, (3)]. In addition, it displays standing waves of complex structure, “turbulence,” and other patterns that must be due to surface physical and chemical mechanisms beyond traditional reaction-diffusion models.

The addition of boundaries allows the study of the influence of different geometries on different aspects of the pattern formation: (i) the elucidation of individual components of the dynamics, for example, by the isolation and study of the behavior of a single traveling pulse or single surface defect; (ii) the controlled study of the interaction between patterns and boundary conditions, such as the “bouncing” of fronts off of walls, or the spatiotemporal resonance

of a wave train with a regular lattice of obstructions; and (iii) the discovery of phenomena that have not been observed on the unbounded surface. Furthermore, experiments in small, simple geometries are amenable to comparisons with theory and simulations.

Despite the importance of the interaction of boundaries with reaction-diffusion patterns, there are only a few experimental attempts in this direction. Observations of reaction-diffusion patterns in simple domains have been made for the homogeneous Belousov-Zhabotinsky reaction [in a ring and a one-dimensional (Couette) reactor] (8) and for nonisothermal catalytic reactions [such as the catalytic oxidation of H_2 on Ni rings, ribbons, and disks (9) and NH_3 oxidation on Pt wires (10)]. Zuburtikudis and Saltsburg (11) used nanofabrication techniques to study finite size effects in the rate of

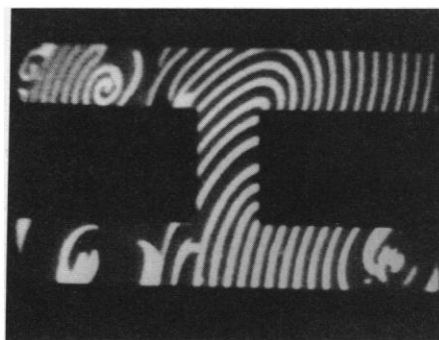


Fig. 1. Spiral and pulse patterns in a large irregular domain; temperature (T) = 440 K, partial pressure of $O_2 = P_{CO} = 5.0 \times 10^{-5}$ mbar, and $P_{O_2} = 4.0 \times 10^{-4}$ mbar. The “H” is 350 μm high.

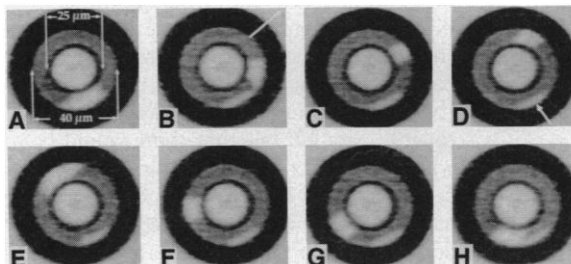


Fig. 2. Traveling CO pulse in a ring; $T = 446$ K, $P_{CO} = 5.6 \times 10^{-5}$ mbar, and $P_{O_2} = 4.0 \times 10^{-4}$ mbar. (A) through (H) represent a temporal progression, with a period of ~ 5 s between panels.

M. D. Graham and I. G. Kevrekidis, Department of Chemical Engineering, Princeton University, Princeton, NJ 08544–5263, USA.

K. Asakura, J. Lauterbach, K. Krischer, H.-H. Rotermund, G. Ertl, Fritz-Haber-Institut der Max-Planck-Gesellschaft, Faradayweg 4-6, 14195 Berlin, Germany.

*Permanent address: Department of Chemical Engineering, University of Wisconsin, Madison, WI 53706, USA.

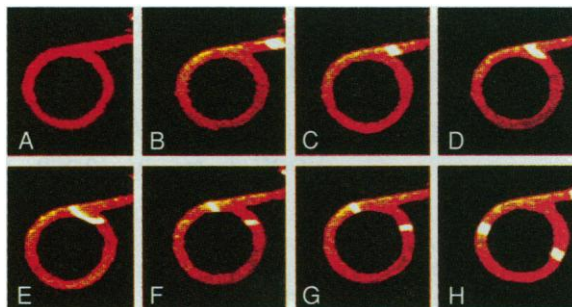
†To whom correspondence should be addressed.

ethane hydrogenolysis at a scale (~ 10 nm) where an altogether different class of electronic and catalytic effects comes into play. Experiments on interactions between reaction-diffusion patterns and inactive domains in the Belousov-Zhabotinsky reaction were first described by Linde and Zirkel (12). The work of Zhabotinsky and co-workers (13) on reflection and refraction of fronts at an interface between two reacting media is the first experimental exploration of these phenomena. For complicated domains, a number of computational papers have recently appeared (14). They model phenomena that range from the interaction of a spiral wave with domain walls to the “diffraction” of pulses passing through orifices.

Carbon monoxide oxidation on Pt exhibits its spontaneous patterns with typical sizes on the order of several (2 to 20) micrometers. The study of mesoscopic spatiotemporal variations in this size range for metal catalyst surfaces, like Pt, has been made possible through the application of spatially resolved surface analysis techniques like photoemission electron microscopy (PEEM) in the late 1980s. In a typical crystal sample of 1 cm by 1 cm, many patterns and many surface defects (such as scratches and dislocations) interact dynamically at any moment. Rather than the analysis of data from such a complicated system, the systematic study of the behavior as its complexity gradually increases is desirable. This study can be done by controlling the ratio of natural and imposed length scales as is routinely done in fluid mechanics (such as experiments in thermal convection at various container sizes), solid-state physics (quantum dots for electron localization), macroscopic reaction-diffusion systems, and computational studies of all of the above.

The experiments were performed on a polycrystalline Pt foil and a Pt(110) single crystal that have also been used in our previous investigations (5, 6). An 80-nm-thick Ti layer was deposited on the Pt surface, and microscopic regions of bare Pt were created by the etching through of the Ti with a negative photoresist process (15). The pattern evolution was followed with a photoemission electron microscope (16), which combines high temporal (25 ms, limited by the video frequency) and spatial (0.1 μm) resolution with a field of view of up to

Fig. 3. Breakup of a CO pulse at a junction; $T = 470$ K, $P_{\text{CO}} = 5.6 \times 10^{-5}$ mbar, and $P_{\text{O}_2} = 4.0 \times 10^{-4}$ mbar. The frames are $150 \mu\text{m}$ by $150 \mu\text{m}$; period between frames is ~ 10 s. White and red indicate predominantly CO-covered and oxygen-covered areas, respectively.



$800 \mu\text{m}$. The contrast in the PEEM images is based on local differences in work function caused by the different adsorbates and adsorbate coverages. In the raw data, oxygen appears dark and CO-rich areas appear lighter gray. The data were recorded on S-VHS videotapes and digitized for further image processing.

We confirmed that in sufficiently large domains (such as $500 \mu\text{m}$ by $500 \mu\text{m}$ squares), the surface reproduces the patterns observed on the macroscopic crystal as well as in polycrystalline samples with grain sizes of a few hundred micrometers (5). A large H-shaped pattern is shown in Fig. 1. The surrounding dark Ti-covered surface is inactive and shows no pattern formation. Spiral waves of different wavelengths can be seen developing. The formation of spiral waves is frequently observed and well investigated on the Pt(110) surface (6). In the straight ($50\text{-}\mu\text{m}$ width) channels propagate reaction-diffusion pulses. This is a case in which the boundaries do not play a very active role in the pattern formation, consistent with the theory of spiral waves in excitable media (2, 3).

We present in Fig. 2 a sequence of snapshots of the progression of a single CO pulse in a ring ($7.5 \mu\text{m}$ thickness, $40 \mu\text{m}$ outer diam-

eter). This is a pronounced example of a pulse in a reaction-diffusion system with anisotropic diffusion: the shape and speed of the pulse change depending on the angle of the front with respect to the crystallographic axes. The axis for faster diffusion is indicated by the arrow in Fig. 2B. The curvature of the leading edge and the trailing edge of the pulse are different. The pulse travels around in ~ 40 s and is not affected by CO partial pressure changes of up to 5%. This pulse was stable for several minutes. The small defect indicated by the arrow in Fig. 2D had no significant influence on the pulse. The light inner circle in Fig. 2 consists of predominantly CO-covered Pt, separated from the ring described above by $3 \mu\text{m}$ of Ti. The overall pattern consisted of several concentric rings, the next of which is partly seen in the figure, also uniformly covered by CO.

In a slightly more complex geometry, the sequence in Fig. 3 shows a CO pulse entering a ring from a synchrotron-like arm. Notice the effect of the curvature of the boundaries on the shape of the pulse as it enters the ring (Fig. 3E), before it breaks in two counterrotating pulses (Fig. 3F).

A case in which the boundaries participate more actively in the pattern selection is illustrated by the four successive snapshots in Fig. 4 of the interaction of a family of pulses with an inert grid. This grid is a square array of $\sim 10\text{-}\mu\text{m}$ -wide Ti islands with a lattice constant of $20 \mu\text{m}$. Locally, one can see the beginnings of multiarmed spirals pinned on the Ti islands. As the rotating arms of the spirals encounter the rows of Ti islands, the lattice tends to slow down and "flatten" the pulses by forcing them to become short arcs connected at cusps. The arrow in Fig. 4 denotes the

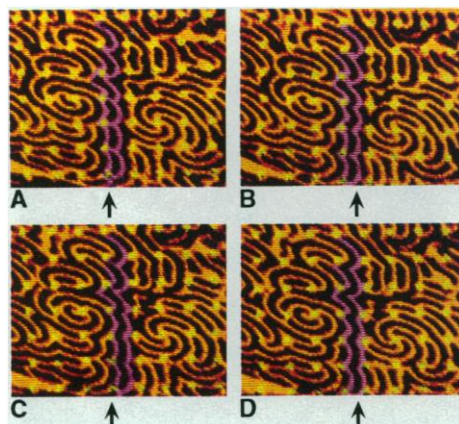


Fig. 4. Pulse patterns in a grid of Ti islands; $T = 425$ K, $P_{\text{CO}} = 2.5 \times 10^{-5}$ mbar, and $P_{\text{O}_2} = 4.0 \times 10^{-4}$ mbar. The frames are $150 \mu\text{m}$ by $120 \mu\text{m}$; ~ 30 s between frames. Orange and brown indicate predominantly CO-covered and oxygen-covered areas, respectively. The Ti islands are light green.

progression of such a pulse (highlighted in purple) moving parallel to the grid: It deforms and heals itself between successive rows. Because pulses tend to be pinned to the grid, the overall pattern conforms to the lattice spacing; we term this behavior "grid resonance" (an average 2:1 ratio resonance is seen in Fig. 4). Sometimes the pulses locally changed their sense of rotation as they encountered a Ti island.

Under certain conditions, very bright regions have been observed by the photoemission electron microscope. These regions have a smaller work function than that of the pure surface and have been interpreted as subsurface oxygen (5, 17). A CO front propagating upward toward the Ti boundary of a Pt circle is shown in Fig. 5A (a CO front appears as the boundary between the light yellow and dark red oxygen-rich areas and propagates into the oxygen-rich region). Subsurface oxygen (bright) appears first in Fig. 5C and is possibly formed from the surface oxygen between the front and the wall. It is subsequently "pushed against the wall" (Fig. 5, D and E) and finally rebounds, emitting a surface oxygen front (Fig. 5, F and G). A quirk of the crystal turned this into a periodic phenomenon: The downward-moving front bounces off an oblique scratch transecting the domain near the position of the front in Fig. 5G. It turns again into a CO front (Fig. 5H), and the procedure repeats itself stably with a period of ~ 2 min. In a related phenomenon, we have observed the bright species (the subsurface oxygen) stably flickering around a defect like a candle flame. The rest of the surface was covered with CO, and no oxygen waves were observed. The flickering showed stable periodic behavior with a period of ~ 2 s.

The last two examples represent cases in which new phenomena are observed in the presence of boundaries. In addition to these, we studied isolated single-surface defects in small ($\sim 5 \mu\text{m}$ by $5 \mu\text{m}$) squares, recorded the rate of "firing" (front nucleation) of these defects, and obtained preliminary results on the dependence of this firing rate on experimental conditions. We also observed the breakup of traveling pulses for certain domain sizes and curvatures.

This exploratory study has revealed a

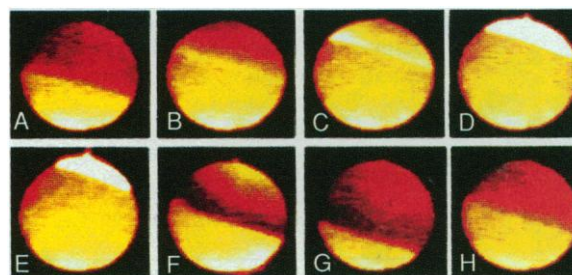


Fig. 5. Front motions in a disk, showing the formation of subsurface oxygen; $T = 457$ K, $P_{\text{CO}} = 2.4 \times 10^{-5}$ mbar, and $P_{\text{O}_2} = 4.0 \times 10^{-4}$ mbar. The frames are $120 \mu\text{m}$ by $170 \mu\text{m}$; ~ 15 s between frames. Light yellow and dark red indicate predominantly CO-covered and oxygen-covered areas, respectively. The bright white color indicates subsurface oxygen.

number of effects that had neither been previously observed in experiments nor predicted by modeling. The setting developed here opens new avenues for the exploration of basic chemistry questions: the nature and number of species involved and their transport mechanisms; the effect of anisotropy; and the effect of dynamic surface reconstructions and of gas-phase coupling. This setting permits the systematic study of pattern formation per se as well as its interactions with domain geometry. The ability to realize elementary geometries will greatly simplify the comparison of simulations and theory with experiments; this should be a serious motivation for further detailed computational and model-building efforts.

REFERENCES AND NOTES

1. Y. Kuramoto, *Chemical Oscillations, Waves and Turbulence* (Springer, Berlin, 1984).
2. R. J. Field and M. Burger, *Oscillations and Traveling Waves in Chemical Systems* (Wiley, New York, 1985).
3. A. S. Mikhailov, *Foundations of Synergetics I* (Springer, Berlin, 1990).
4. A. T. Winfree, *Chaos* **1**, 303 (1991); G. Ertl, *Science* **254**, 1750 (1991); J. E. Pearson, *ibid.* **261**, 189 (1993); K. J. Lee, W. D. McCormick, Q. Ouyang, H. L. Swinney, *ibid.*, p. 192.
5. J. Lauterbach, G. Haas, H.-H. Rotermund, G. Ertl, *Surf. Sci.* **294**, 116 (1993).
6. S. Nettesheim, A. von Oertzen, H.-H. Rotermund, G. Ertl, *J. Chem. Phys.* **98**, 9977 (1993).
7. H.-H. Rotermund, W. Engel, M. Kordesch, G. Ertl, *Nature* **343**, 355 (1990); H.-H. Rotermund, *Surf. Sci.* **283**, 87 (1993); *Phys. Scr. Top. Conf.* **49**, 549 (1993).
8. Z. Noszticzius *et al.*, *Nature* **329**, 619 (1987); V. Castets, E. Dulos, J. Boissonade, P. DeKepper, *Phys. Rev. Lett.* **64**, 2953 (1990); W. Y. Tam and H. L. Swinney, *Physica D* **46**, 10 (1990).
9. G. Philippou, F. Schultz, D. Luss, *J. Phys. Chem.* **95**, 3224 (1991); S. L. Lane, M. D. Graham, D. Luss, *Am. Inst. Chem. Eng. J.* **39**, 1497 (1993); S. L. Lane and D. Luss, *Phys. Rev. Lett.* **70**, 830 (1993).
10. G. A. Cordonier and L. D. Schmidt, *Chem. Eng. Sci.* **44**, 1983 (1989).
11. I. Zuburtikudis and H. Saltsburg, *Science* **258**, 1337 (1992).
12. H. Linde and C. Zirkel, *Z. Phys. Chem.* **174**, 145 (1991).
13. A. M. Zhabotinsky, M. D. Eager, I. R. Epstein, *Phys. Rev. Lett.* **71**, 1526 (1993).
14. A. M. Pertsov, E. A. Ermakova, E. E. Shnol, *Physica D* **44**, 178 (1990); A. Babloyantz and J. A. Sepulchre, *ibid.* **49**, 52 (1991); J. A. Sepulchre and A. Babloyantz, *Phys. Rev. E* **48**, 187 (1993).
15. The sample was transferred into an ultrahigh vacuum chamber, and the surface was cleaned by standard procedures. Throughout the reaction, its temperature was kept constant to within 0.1 K. An inert thin layer of TiO₂ forms on the surface of the Ti mask.
16. W. Engel, M. E. Kordesch, H.-H. Rotermund, S. Kubala, A. von Oertzen, *Ultramicroscopy* **36**, 148 (1991).
17. J. Lauterbach, K. Asakura, H.-H. Rotermund, *Surf. Sci.*, in press; H.-H. Rotermund, J. Lauterbach, G. Haas, *J. Appl. Phys. A* **57**, 507 (1993).
18. We thank S. Forrest and M. Lange for sample preparation. Supported partially by the Advanced Research Projects Agency—Office of Naval Research, the National Science Foundation, the David and Lucile Packard Foundation, and the Alexander von Humboldt Foundation.

22 October 1993; accepted 21 January 1994

Crystal Structure of the Principal Neutralization Site of HIV-1

Jayant B. Ghiara, Enrico A. Stura, Robyn L. Stanfield, Albert T. Profy, Ian A. Wilson*

The crystal structure of a complex between a 24-amino acid peptide from the third variable (V3) loop of human immunodeficiency virus-type 1 (HIV-1) gp120 and the Fab fragment of a broadly neutralizing antibody (59.1) was determined to 3 angstrom resolution. The tip of the V3 loop containing the Gly-Pro-Gly-Arg-Ala-Phe sequence adopts a double-turn conformation, which may be the basis of its conservation in many HIV-1 isolates. A complete map of the HIV-1 principal neutralizing determinant was constructed by stitching together structures of V3 loop peptides bound to 59.1 and to an isolate-specific (MN) neutralizing antibody (50.1). Structural conservation of the overlapping epitopes suggests that this biologically relevant conformation could be of use in the design of synthetic vaccines and drugs to inhibit HIV-1 entry and virus-related cellular fusion.

The V3 loop of HIV-1 gp120 plays a critical role in viral infectivity and tropism and contains the principal neutralizing determinant (PND) of HIV-1 viruses. Neutralizing antibodies to the V3 loop can inhibit viral entry even after gp120 has bound CD4, the primary receptor for the virus (1). Syncytia formation, a result of the fusion of CD4-positive cells with infected cells expressing gp120, is also inhibited by these antibodies. Furthermore, mutations in the V3 loop give rise to noninfectious viruses that can still bind CD4 (2), indicating that the V3 loop is important for subsequent membrane fusion events. It has been proposed that binding or cleavage of the V3 loop by secondary receptors (3, 4) may be required for pH-independent membrane fusion and viral entry (5).

The amino acid sequence of the PND is highly variable, except for a short stretch at the crown or tip of the V3 loop (6). Several lines of evidence already indicate that this region may adopt a conserved structure in different HIV-1 isolates. The Gly-Pro-Gly-Arg sequence, found in most North American and European isolates, occurs more frequently than any other in known type II β turns (7), and proton nuclear magnetic resonance (NMR) techniques have indicated a preference for a β -turn conformation in synthetic V3 peptides (8). A secondary structure prediction has further suggested that the V3 loop adopts a β -hairpin structure (β -strand-type II β -turn- β -strand motif), with a short helix at its carboxyl end (6).

Despite the sequence (and possible structural) conservation at the crown of the

V3 loop, hypervariable flanking sequences cause mainly type-specific neutralizing antibodies to be generated against the various strains of HIV-1. Passive immunization with such a type-specific anti-V3 monoclonal antibody (mAb) has been shown to protect chimpanzees from individual strains of the virus (9). Furthermore, antibodies that primarily recognize the conserved crown of the V3 loop have recently been shown to effect a broad neutralization of different HIV-1 isolates (10, 11). A three-dimensional structure for this V3 loop region could then be used in the design of more effective synthetic vaccines and, possibly, of inhibitors of the membrane fusion process.

As a structure for gp120 is not yet available, we investigated the structural features of the HIV-1 PND by determining the conformation of PND peptides in complex with neutralizing mAbs that bind overlapping epitopes within the V3 loop.

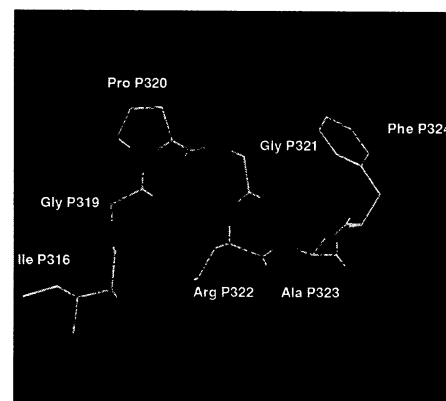


Fig. 1. $F_o - F_c$ omit electron density for the bound peptide. The density at 2.7σ is shown only around the S-shaped double turn formed by residues Gly-Pro-Gly-Arg-Ala-Phe. Peptide residue numbers are according to the BH10 isolate sequence (12), preceded by the letter P.

J. B. Ghiara, E. A. Stura, R. L. Stanfield, I. A. Wilson, Department of Molecular Biology, The Scripps Research Institute, 10666 North Torrey Pines Road, La Jolla, CA 92037, USA.
A. T. Profy, Repligen Corporation, Cambridge, MA 02139, USA.

*To whom correspondence should be addressed.